Accepted Preprint first posted on 31 October 2016 as Manuscript JOE-16-0370

10-13-16

Muscle injury and impaired function, and insulin resistance in Chromogranin A knockout mice

By

Kechun Tang[2], Teresa Pasqua[2], Angshuman Biswas[2], Sumana Mahata[3], Jennifer Tang[2], Alisa Tang[2], Gautam K. Bandyopadhyay[2], Amiya P. Sinha-Hikim[4, 5], Nai-Wen Chi[1,2], Nicholas J.G. Webster[1,2], Angelo Corti[6], Sushil K. Mahata[1,2]

[1]VA San Diego Healthcare System, San Diego, California, USA; [2]Department of Medicine, University of California, San Diego, La Jolla, California, USA; [3]Division of Biology & Biological Engineering, California Institute of Technology, Pasadena, California, USA; [4]Charles Drew University of Medicine and Science, Los Angeles, USA; [5]David Geffen School of Medicine, University of California-Los Angeles, Los Angeles, California, USA; [6]IRCCS San Raffaele Scientific Institute, San Raffaele Vita-Salute University, Milan, Italy.

The authors have nothing to declare

Short title: Chromogranin A regulates muscle function

Author for correspondence:
Sushil K. Mahata, Ph.D.
Metabolic Physiology & Ultrastructural Biology Laboratory
Department of Medicine
University of California, San Diego (0732)
9500 Gilman Drive
La Jolla, CA 92093-0732
Tel: (858) 552-8585, ext. 2637
Email: smahata@ucsd.edu

Key words: Skeletal muscle, insulin signaling, glucose metabolism, tubular aggregates, and mitochondria

Abstract

Chromogranin A (CgA) is widely expressed in endocrine and neuroendocrine tissues as well as in the central nervous system. We observed CgA expression (mRNA and protein) in the gastrocnemius (GAS) muscle and found that performance of CgA-deficient *Chga*-KO mice in treadmill exercise was impaired. Supplementation with CgA in *Chga*-KO mice restored exercise ability suggesting a novel role for endogenous CgA in skeletal muscle function. *Chga*-KO mice display (i) lack of exercise-induced stimulation of pAKT, pTBC1D1 and phospho-p38 kinase signaling, (ii) loss of GAS muscle mass, (iii) extensive formation of tubular aggregates (TA), (iv) disorganized cristae architecture in mitochondria, (v) increased expression of the inflammatory cytokines *Tnfα, Il6* and *Ifnγ*, and fibrosis. The impaired maximum running speed and endurance in the treadmill exercise in *Chga*-KO mice correlated with decreased glucose uptake and glycolysis, defects in glucose oxidation and decreased mitochondrial cytochrome C oxidase activity. The lack of adaptation to endurance training correlated with the lack of stimulation of p38MAPK that is known to mediate the response to tissue damage. Since CgA sorts proteins to the regulated secretory pathway, we speculate that lack of CgA could cause misfolding of membrane proteins inducing aggregation of sarcoplasmic reticulum (SR) membranes and formation of tubular aggregates that is observed in *Chga*-KO mice. In conclusion, CgA deficiency renders the muscle energy deficient, impairs performance in treadmill exercise and prevents regeneration after exercise-induced tissue damage.

Introduction

Chromogranin A (CgA), the secretory proprotein of chromaffin granules, is widely expressed in endocrine and neuroendocrine tissues as well as in the central nervous system (Winkler and Fischer-Colbrie 1992; Montero-Hadjadje, et al. 2008; Bartolomucci, et al. 2011). CgA is processed to multiple biologically active peptides including pancreastatin (Tatemoto, et al. 1986; Sanchez-Margalet, et al. 2010), vasostatin I (Aardal, et al. 1993; Tota, et al. 2008), catestatin (Mahata, et al. 1997; Mahata, et al. 2003; Mahapatra, et al. 2005; Angelone, et al. 2008), and serpinin (Tota, et al. 2012). The CgA protein was initially detected in the large dense-core vesicles of sympathetic nerves and in the brainstem, which is rich in adrenergic neurons (Banks, et al. 1969; De Potter, et al. 1970a; Bartlett, et al. 1976). Therefore, it was assumed that CgA is an adrenergic protein confined to the sympathetic nerve (Banks et al. 1969; De Potter, et al. 1970b; Bartlett et al. 1976) and to the adrenal medulla (Helle 1966; Smith and Winkler 1967; Smith and Kirshner 1967). Subsequently CgA was also detected in cholinergic motor neurons of the spinal cord (Somogyi, et al. 1984) and in cholinergic nerve terminals in the muscles of the diaphragm (Volknandt, et al. 1987). These latter findings suggested that CgA might influence skeletal muscle function and indeed CgA knockout mice display impaired skeletal muscle function in addition to hyperadrenergic (Mahapatra et al. 2005), hypertensive (Mahapatra et al. 2005) and insulin sensitive phenotypes (Gayen, et al. 2009).

During exercise, the muscle's increased need for energy is compensated by increasing uptake and utilization of glucose as the primary energy source (Goodyear and Kahn 1998). Both exercise and insulin increase glucose uptake in skeletal muscle through the translocation of the Glut4 glucose transporter from an intracellular compartment to the surface of the cell in response to activation of the Rab GTPase TBC1D1 (Douen, et al. 1989; Hirshman, et al. 1990; Goodyear, et al. 1991a; Goodyear, et al. 1991b). Muscle contraction recruits Glut4 to the plasma membrane independently of insulin in rat skeletal muscle, suggesting alternative but convergent signaling (Goodyear, et al. 1990). Therefore, a combination of exercise and insulin can exert additive effects on glucose transport.

Exercise injures skeletal muscle by damaging the attachment of myofibrils to the extrasarcolemic cytoskeleton (Friden, et al. 1991), and evoking an inflammatory response (Paulsen, et al. 2013). A number of intracellular mechanisms contribute to muscle damage including calcium overload, reactive oxygen species

(ROS) production and a decrease in cellular ATP (Armstrong, et al. 1991). This fall in ATP levels in response to exercise stress (Perrey and Rupp 2009) activates Pgc1α, AMPK and p38MAPK kinase signaling to allow cells to adapt (Gibala 2009). This post-exercise response involves mitochondrial biogenesis concomitant with the onset of muscle fiber differentiation (Duguez, et al. 2002; Gibala 2009). Regeneration of muscle fibers takes place through the activation of quiescent muscle precursor cells, the formation of proliferating progenitor satellite cells leading to fusion into differentiated myofibers (Wagers and Conboy 2005). The intermediate progenitor cells express MyoD and myogenic transcription factor Pax3, and asymmetrically divide and differentiate into myoblasts expressing Pax3, Myf-5 and desmin (Conboy and Rando 2002). The activation of satellite cells under the basal lamina of muscle fibers is accelerated by insulin-like growth factor-I and mechano-growth factor induced in exhausted muscles after training (Machida and Booth 2004; Schiaffino and Mammucari 2011).

Exercise-induced muscle pain, stiffness, and cramping are caused by enzyme deficiencies such as myophosphorylase deficiency and phosphofructokinase deficiency leading to metabolic defects (Tarui, et al. 1965; Layzer, et al. 1967; Cornelio and Di Donato 1985). Both deficiencies are accompanied by reduced anaerobic glycolysis resulting in reduced levels of muscle lactate production, higher serum creatine phosphokinase levels, and the presence of histological tubular aggregates (TA) in type-II muscle fibers (Bertorini, et al. 1977; Korenyi-Both, et al. 1977). TAs are ordered arrays of cylindrical sarcoplasmic reticulum (SR) tubules that are observed in many skeletal muscle myopathies (Boncompagni, et al. 2012). Experimental inhibition of glycolysis with iodoacetate produces a similar muscle phenotype (Brumback, et al. 1980) and these TAs have been found in other experimental models including extreme hypoxia in rats (Schiaffino, et al. 1977) and the deficiency of dystrophin (Craig and Allen 1980), or Caveolin-1 or -2 (Schubert, et al. 2007) in mice. The formation of TAs in injured muscle fibers may be associated with exercise-induced muscle pain (Brumback, et al. 1981). Accumulation of calsequestrin, a sarcoplasmic reticulum (SR) Ca^{2+} binding protein, triggers TA formation through swelling of free SR cisternae and extension of the enlarged SR sacs into multiple, longitudinally oriented tubules with SERCA (sarcoplasmic reticulum Ca^{2+}-ATPases) in the membrane and calsequestrin in the lumen (Boncompagni et al. 2012).

We have previously shown hepatic insulin sensitivity but muscular insulin resistance in *Chga*-KO mice (Gayen et al. 2009). Here we show impaired muscle function, muscle fiber degeneration and decreased insulin signaling coupled with attenuated glucose uptake and metabolism in *Chga*-KO skeletal muscle. In addition, at

the ultrastructural level, we found the presence of TAs in gastrocnemius muscle of *Chga*-KO mice. Treatment of *Chga*-KO mice with CgA for 15 days restored muscle performance, which establishes a novel role of CgA in regulation of skeletal muscle function.

Materials and Methods

Animals

Adult (5-6 months old) male *Chga*-KO mice on a mixed genetic background (50% 129svJ; 50% C57BL/6J) and wild-type C57BL/6J mice were studied. Mice were kept on a 12 hr dark/light cycle, and fed *ad libitum* with a normal chow diet (NCD: 14% calories from fat; LabDiet 5P00). The Institutional Animal Care and Use Committee of the University of California San Diego approved all procedures.

Immunoblotting

Tissues were homogenized in a lysis buffer containing phosphatase and protease inhibitors. Homogenates were subjected to 10% SDS-PAGE and immunoblotted. The following primary antibodies were obtained from Cell Signaling Technology (Boston, MA): AKT and pS473-AKT (rabbit polyclonal at 1:1000 dilution), AMPK and pT172-AMPKa (rabbit polyclonal at 1:1000 dilution), P38 and pT180/Y182-P38 (rabbit polyclonal at 1:1000 dilution), TBC1D1, pT590-TBC1D1 and pS700-TBC1D1 (rabbit polyclonal at 1:500 dilation). Anti-CgA ($hCgA_{352-372}$) polyclonal antibody was raised in rabbit by a commercial vendor Sdix Inc. (Newark, DE) and used at a dilution of 1:1000. This antibody detected full-length CgA (75 kDa), proteoglycan form of CgA (90 kDa), and proteolytically processed CgA (49 kDa and 30 kDa). In addition, we also used anti-CgA mouse monoclonal antibody 5A8 (epitope $hCgA_{R47-L57}$) (Ratti, et al. 2000) at a dilution of 1:1000 that cross-reacts with murine CgA (Colombo, et al. 2002).

Real-time RT-PCR assay for measurement of target mRNAs

Total cellular RNA from GAS was isolated with TriPure Isolation Reagent (Invitrogen) and purified and DNase I treated with RNAeasy Mini Kit (Qiagen Inc. Valencia, CA). Either a Thermoscript kit (Invitrogen) or a qScript CDNA synthesis kit (Quantabio, Beverly, MA) was used for reverse transcription from total RNA. The RT products were amplified either with an RT2 Real-Time SYBR Green Kit (AuperArray, Fredrick, MD) or PERFECTA SYBR FASTMIX L-ROX 1250 (Quantabio, Beverly, MA). PCR reactions were run either on a MxP3000 Real-Time PCR system (Stratagene, La Jolla, CA) or an Applied Biosystems 7500 Fast Real-Time

PCR system (Foster City, CA). All PCRs were normalized to *Gapdh*, and relative expression levels were determined by the $\Delta\Delta C_t$ method. Primer sequences are provided in Table 1.

2-deoxy-glucose (2DG) uptake and glucose metabolism.

In vivo glucose uptake and production of glucose-6-phosphate (G6P) was carried out essentially as described by Crosson et al. (Crosson, et al. 2003) but using double isotopes ^{3}H-glucose and ^{14}C-2-deoxyglucose (2DG). To evaluate glucose uptake in GAS and formation of G6P *in vivo*, we injected a cocktail of ^{3}H-glucose and ^{14}C-2DG in 25% glucose solutions into sedentary WT and *Chga*-KO mice and looked at the uptake and metabolism after 90 min of injection. Since some glucose is trapped in extracellular and interstitial space, which may give an overestimation of uptake, we estimated the contribution of extracellular space to the uptake in each tissue by ^{14}C-mannitol incorporation. Blood glucose was measured at 0 and 90 minutes after glucose injection. Mice were then sacrificed and tissues were dissected and frozen rapidly in liquid nitrogen. We determined ^{3}H-glucose and ^{14}C-2DG specific activities in blood samples. Tissue homogenates were deproteinized and neutralized, then the radioactivity in the supernatants was counted before and after passing through an anion exchange resin to remove 2-DG-6-phosphate (2DG6P) and G6P. The difference in radioactivity before and after resin treatment represents the amount of 2DG6P and G6P formed. We counted both ^{3}H and ^{14}C. We expect that ^{14}C will represent 2DG uptake and ^{3}H counts will represent glucose uptake as well as the extent of further metabolism (glycolysis and oxidation) and glycogen formation. Glucose metabolism was determined by the difference of 2DG6P and G6P. For treadmill endurance exercises, mice were run at a speed of 22 meter/min for 20 min per day for 15 days followed by immediate injection with ^{3}H-glucose and ^{14}C-2DG in 25% glucose solutions for determination of 2DG uptake and metabolism 90 minutes after glucose injection.

Palmitate uptake and metabolism

To determine uptake of palmitic acid in GAS in vivo and formation of acid soluble metabolite (ASM), we injected 100 µl solution of U-^{14}C-palmitic acid-BSA complex (molar ratio 2.5:1), containing 1 µCi and 250 µM palmitate, into sedentary WT and *Chga*-KO mice, and looked at the uptake and metabolism after 90 min of injection. For treadmill endurance exercise, mice were run at a speed of 22 meter/min for 20 min per day for 15

days followed by immediate injection of 100 µl solution of U-^{14}C-palmitic acid-BSA complex. After 90 minutes, mice were sacrificed, blood was saved and tissues were put into a mixture of chloroform:methanol:water (1:2:0.8 vol/vol). Tissues were homogenized and centrifuged (10,000x g for 10 min). The pellets were used for protein assay after dissolving in 2N NaOH at 60˚C for 1 hour. To the supernatants, 0.25 ml chloroform and 0.5 ml 1M NaCl in 1M HCl were added and the mixtures were vortexed vigorously and centrifuged (10000x g, 10 min) to separate two clear layers. The lower chloroform layers containing all lipids were collected in scintillation vials, dried overnight and counted. This radioactivity represents the amount of fatty acids taken up by the tissue. Fatty acid concentration and radioactivity in the saved serum were determined to calculate specific activity of the radioactive fatty acid in serum. Oxidation of radioactive fatty acids is represented by the radioactivity in CO2 formed and by the radioactivity in the acid-soluble materials (ASM) in the acidified supernatants. We only measured ASM for this work (did not measure $^{14}CO_2$ formation). The upper acidic aqueous layers were neutralized and counted.

Endurance tests

WT and *Chga*-KO mice were exercised on an Omnipacer Treadmill LC4 (Omnitech Electronics, Inc., Columbus, OH) on a 10° incline while breathing room air. Subjecting mice to an incremental speed running test determined the maximal running capacity. Thus, mice were initially exercised at a speed of 24 m/min with increments of 2 m/min every 30 sec until exhaustion. To determine endurance capacity, mice were run on a treadmill at 20 m/min (60% of the average maximal speed of *Chga*-KO mice) at 10° inclination until exhaustion, which was defined as consistent refusal to run despite contact with the electrical grid at the rear of the treadmill. To find out the role of CgA in endurance exercise, *Chga*-KO mice were supplemented with recombinant CgA (0.05 µg/g BW, IP daily for 15 days) and tested their abilities in endurance exercise. Full-length human CgA1-439 was prepared by recombinant DNA technology in Angelo Corti's laboratory as described previously (Crippa, et al. 2013).

Light and Transmission Electron Microscopy (TEM)

Mice were deeply anesthetized and the gastrocnemius (GAS) muscles were perfusion fixed through the left ventricle. Mice were flushed with a pre-warmed (37°C) calcium and magnesium free buffer, which is

composed of DPBS (Life Technologies Inc. Carlsbad, CA), 10 mM HEPES, 0.2 mM EGTA, 0.2% bovine serum albumin, 5 mM glucose and 10 mM KCl for 3 min followed by perfusion with freshly prepared pre-warmed (37°C) fixative containing 2.5% glutaraldehyde, 2% paraformaldehyde in 0.15 M cacodylate buffer for 3 min using a peristaltic pump (5 ml/min; Langer Instruments Corp, Boonton, NJ). GAS muscles were dissected out and put in the same fixative overnight (2 hrs at room temperature and 12 hrs at 4°C), and postfixed in 1% OsO_4 in 0.1 M cacodylate buffer for 1 hour on ice. The tissues were stained *en bloc* with 2-3% uranyl acetate for 1 hour on ice. The tissues were dehydrated in graded series of ethanol (20-100%) on ice followed by one wash with 100% ethanol and two washes with acetone (15 min each) and embedded with Durcupan. Longitudinal and transverse sections were cut at 50 to 60 nm on a Leica UCT ultramicrotome, and picked up on Formvar and carbon-coated copper grids. Sections were stained with 2% uranyl acetate for 5 minutes and Sato's lead stain for 1 minute. Grids were viewed using a JEOL 1200EX II (JEOL, Peabody, MA) TEM and photographed using a Gatan digital camera (Gatan, Pleasanton, CA). Micrographs were randomly taken from 3 GAS each from WT and *Chga*-KO mice, which were fixed and processed in two different days.

Morphometric analysis

Samples were blinded and 2 people did measurements randomly from different cells as described previously (Pasqua, et al. 2016). The free-hand tool in NIH ImageJ 1.49 software was used to manually trace around the cristae membrane, mitochondrial outer membrane area and cytoplasm area for determination of the mitochondrial and cristae volume density. The sum of the area of the total complement of cristae represented the cristae membrane surface area. To normalize the measurement, this area was divided by the outer membrane area per mitochondrion. The sum of the area of the mitochondria was divided by the area of the cytoplasm and multiplied by 100 to determine the mitochondrial volume density (%). For determination of the cristae volume density (%), the sum of the area of the cristae was divided by the outer area of the mitochondria and multiplied by 100, as described previously (Pasqua et al. 2016).

Data presentation and statistical analysis

Data are expressed as mean ± SEM. Statistics were performed with GraphPad Prism 7 software (GraphPad software, Inc, La Jolla, CA). Data were analyzed with one-way ANOVA or 2-way ANOVA followed by multiple comparison tests where appropriate. Additionally, we performed unpaired Student's *t* tests with Welch's correction when appropriate. Statistical significance was defined as $p<0.05$.

Results

Loss of CgA impairs muscle performance. Although *Chga*-KO mice are 13% heavier than WT mice (Fig. 1a), the GAS muscle showed a 10% decrease in weight compared to WT mice (Fig. 1b). *Chga*-KO mice showed a 37% decrease in maximum running speed compared to WT mice (Fig. 1c) and also showed 48% decrease in endurance as measured by time to exhaustion (Fig. 1d). We then tested whether supplementation of CgA to *Chga*-KO mice would restore muscle function. We found that CgA supplementation restored both maximal capacity (Fig. 1e) and endurance performance (Fig. 1f) in *Chga*-KO mice, indicating an important role for CgA in skeletal muscle function. With the profound effect on exercise performance and muscle mass, we wondered whether CgA is expressed in GAS muscle. Western blot analyses with a CgA antiserum ($hCgA_{352-372}$) confirmed CgA expression in GAS muscle (Fig. 1d). As positive controls, we used adrenal and pituitary glands, which showed major bands at 75 and 100 kDa, respectively. Like the pituitary gland, GAS muscle showed a CgA proteoglycan band at 100 kDa. In addition, adrenal and pituitary glands showed a proteolytically processed band at 49 kDa but GAS muscle showed a 30 kDa fragment (Fig. 1g). Western blot analyses with anti-CgA mouse monoclonal antibody 5A8 (epitope $hCgA_{47-57}$) (Ratti et al. 2000) capable of cross-reacting with murine CgA (Colombo et al. 2002) confirmed CgA expression in GAS muscle (Fig. 1h). Both CgA protein (Fig. 1h) and *Chga* mRNA (Fig. 1i) were undetectable in *Chga*-KO mice. We have also detected *Chga* mRNA in GAS muscle (Fig. 1j). Amongst the tissues tested (GAS muscle, adrenal gland, pituitary gland, hypothalamus, and pancreatic islets), *Chga* expression appears to be lowest in GAS muscle (Fig. 1h-j). We also looked at the expression of other members of the Chromogranin/Secretogranin protein family (*Chgb* and *Scg2)*, which revealed that multiple granins were detected, with *Scg2* being the most highly expressed granin (Fig. 1i-n).

Insulin-induced signaling. Previously we have shown muscle insulin resistance in *Chga*-KO mice (Gayen et al. 2009). Hence, we tested whether insulin signaling was impaired in GAS from *Chga*-KO mice. Insulin caused 2.2- and 1.7-fold increments in AKT (Ser473) phosphorylation in WT mice and *Chga*-KO mice, respectively (Fig. 2a&b); indicating impaired PI-3Kinase signaling in GAS muscle. Insulin also activates the stress-activated p38MAPK (Somwar, et al. 2000), so we evaluated insulin-induced activation of p38MAPK. Insulin-induced phosphorylation of p38K was also significantly higher in WT mice than *Chga*-KO mice (2.0 versus 1.5-fold,

253 respectively), indicating a similar impairment in MAPK signaling pathway (Fig. 2a&d). The TBC1D1 protein
254 plays an important role in insulin and exercise-regulated Glut4 translocation (Sakamoto and Holman 2008;
255 Middelbeek, et al. 2013) and AKT phosphorylates TBC1D1 at Thr590 in skeletal muscle (Vichaiwong, et al.
256 2010). Consistent with the AKT data, insulin increased phosphorylation of TBC1D1 at Thr590 2.6-fold in WT
257 mice but not in *Chga*-KO mice, indicating a defect downstream of AKT in insulin signaling in *Chga*-KO mice (Fig.
258 2a&c).
259
260 **Exercise-induced signaling.** Exercise activates both AMPK (AMP-activated protein kinase), which is sensitive
261 to the AMP/ATP ratio, and AKT in skeletal muscle (Sakamoto, et al. 2003) (Richter and Ruderman 2009). Both
262 activated AKT and AMPK phosphorylate TBC1D1 but at distinct residues (Thr590 and Ser700, respectively)
263 (Vichaiwong et al. 2010). Therefore, we assessed whether the impaired muscle function during exercise in
264 *Chga*-KO mice is associated with impaired AKT or AMPK activation and phosphorylation of TBC1D1. While
265 exercise caused 1.6-fold increase in phosphorylation of AKT at Ser473, it had no effect on AKT phosphorylation
266 in *Chga*-KO mice (Fig. 3a&b). In contrast, exercise stimulated phosphorylation of AMPKα at Thr172 site was
267 unchanged (1.5-fold in both WT and *Chga*-KO) (Fig. 3a&c). Although exercise stimulated phosphorylation of
268 TBC1D1 at Thr590 1.4-fold (AKT site) and at Ser700 1.5-fold (AMPK site) in WT muscle, it had no effect on
269 TBC1D1 phosphorylation in muscle from *Chga*-KO mice. These findings indicate that both AKT and AMPK-
270 mediated phosphorylation of TBC1D1 is compromised in *Chga*-KO mice. Exercise also activates p38MAPK in
271 humans (Aronson, et al. 1997; Osman, et al. 2000) and rats (Goodyear, et al. 1996). Here, we found complete
272 abolition of exercise-induced phosphorylation of p38MAPK in *Chga*-KO-GAS (Fig. 3a&f), suggesting that the
273 adaptation mechanism to exercise–induced stress and damage has been compromised in *Chga*-KO-GAS.
274
275 **Glucose and fatty acid uptake and metabolism in response to exercise.** In skeletal muscle, insulin and
276 exercise are the most physiologically relevant stimulators of glucose transport via the translocation of Glut4 from
277 intracellular depots to the sarcolemma and transverse tubules (Lauritzen, et al. 2010). Activated AKT and
278 AMPK phosphorylate TBC1D1 and activate its GTPase activity allowing Glut4 vesicle translocation. Although
279 blood glucose levels were comparable between WT and *Chga*-KO mice (Fig. 4a), the expression of *Glut4* was
280 significantly reduced in *Chga*-KO GAS muscle (Fig. 4c). Endurance exercise stimulated both uptake of 2DG (by

1.8-fold) and utilization of G6P (by 1.6-fold) in WT mice, but both glucose uptake and utilization of G6P were decreased in the sedentary *Chga*-KO mice and did not change significantly with exercise (Fig. 4b&d). Decreased G6P content indicates increased glucose utilization. *Chga*-KO mice displayed decreased plasma triglycerides (Fig. 4e) and dramatically reduced expression of the fatty acid transporter *Cd36* (Fig. 4g). Glucose and fatty acids are the main substrates that provide metabolic energy for the contractile activity of muscle. Although glucose uptake and metabolism were increased in WT muscle after endurance exercise, fatty acid uptake and metabolism were decreased (Fig. 4f) consistent with a switch from lipid oxidation to glucose utilization in GAS muscle. Similar to the findings for glucose utilization, sedentary *Chga*-KO mice showed decreased fatty acid uptake and oxidation, endurance exercise caused a further drop in fatty acid uptake and metabolism (Fig. 4h). Taken together these findings indicate that GAS muscle in *Chga*-KO mice shows impaired utilization of both glucose and fatty acids as an energy source.

Expression of genes involved in regeneration and inflammation: We assessed a panel of muscle progenitor and satellite cell markers in GAS muscle from WT and *Chga*-KO mice. In sedentary mice, we found increased expression of progenitor cell markers *MyoD* (4-fold) and *Pax3* (3.4-fold) in *Chga*-KO mice compared to WT mice (Fig. 5a) but no change in satellite marker *Myf5* (Relaix, et al. 2006; Young and Wagers 2010; Filareto, et al. 2015). *Chga*-KO mice also showed increased expression of pro-inflammatory genes *Tnfα* (1.8-fold), *Ifnγ* (3.8-fold), and *Il6* (7.3-fold) as well as expression of anti-inflammatory gene *Il10* (by 5.6-fold) as compared to WT mice (Fig. 5b). It is possible that while the increased expression of *MyoD1* and *Pax3* may drive proliferation and differentiation of progenitor cells (Relaix et al. 2006; Young and Wagers 2010; Filareto et al. 2015), increased expression of *Ifnγ* may inhibit myogenin activity and prevent differentiation (Londhe and Davie 2011).

Ultrastructural analysis of GAS muscle in sedentary mice

Hematoxylin/eosin staining of transverse sections of GAS muscle revealed morphological alterations in *Chga*-KO mice compared to WT (Fig. 6a&b). In particular, the sections from *Chga*-KO mice showed increased intermyofibrillar fibrosis as shown by increased expression of collagen type 1 alpha 1 (*Col1a1)*, collagen type III alpha 1 (*Col3a1)*, lysyl oxidase (*Lox)*, fibronectin 1 (*Fn1)*, and smooth muscle alpha-actin (*Acta2)* (Fig. 6 c-h)

and the demonstration of collagen fibers at the ultrastructural level (Fig. 6i-k). In addition, histological sections show central nucleation, smaller rounded fibers and unusual irregular clusters of dotted structures in the myofibrillar region suggesting tubular aggregation (Fig. 6a&b). These alterations prompted us to examine those structures at the ultrastructural level.

In WT mice, we observed a mitochondrion in the intermyofibrillar (IMF) region on either side of the Z-disc (perpendicular to the Z-disc) in longitudinal sections (Fig. 7a&b). In addition, we found triads consisting of T-tubules (TT) flanked by smooth sarcoplasmic reticulum (SSR) adjacent to the mitochondria (Fig. 7b&c). In contrast, these IMF structures were disrupted in *Chga*-KO-GAS with fewer or absent mitochondria, and smaller triad structures (Fig. 7d,e&f). In place of these IMF mitochondria, glycogen granules were detected either on one or both sides of the Z-disc in sedentary *Chga*-KO-GAS. Morphometric analysis of structures in *Chga*-KO-GAS indicated decreased mitochondrial density and area (Fig. 7g&h). However, there were no significant changes in cristae density or area for the remaining mitochondria (Fig. 7i&j). Defective mitochondrial function in sedentary *Chga*-KO-GAS was observed by the decreased cytochrome C oxidase (CCO) activity compared to WT mice (Fig. 7k). Subsarcolemmal mitochondria (SSM) displayed prominent cristae in WT mice (Fig. 8a&b), but SSM mitochondria were smaller in size and with fewer cristae in *Chga*-KO mice (Fig. 8c&d). In addition, we observed mitophagy, and inclusion body and glycogen granules in the subsarcolemmal region in *Chga*-KO mice (Fig. 8c&d).

We also examined the ultrastructure of exercised muscle. IMF mitochondria in exercised WT mice were enlarged but maintained their localization perpendicular to the Z-disc (Fig. 9a), whereas exercised *Chga*-KO-muscle showed decreased numbers of mitochondria and increased observation of tubular aggregates (TA) (Fig. 9b). Higher magnification revealed dilated cristae in both the SSM and IMF mitochondria of WT mice, (Fig. 9c&e) but mitochondria in exercised *Chga*-KO mice displayed smaller round or ovoid cristae (Fig. 9d&f).

In WT mice, tubular aggregates (TAs) were not detected in the subsarcolemmal as well as myofibrillar regions in transverse sections (Fig. 10a&b). As compared to longitudinal sections, mitochondria in the myofibrillar regions appear elongated and connected in transverse sections (Fig. 10a&b). In contrast to WT mice, TAs were observed in sedentary *Chga*-KO mice in both transverse (Fig. 10c&d) and longitudinal (Fig. 10e&f) sections. In addition, TAs are detected both in the subsarcolemmal (Fig. 10c&e) and myofibrillar (Fig. 10d&f) regions. TAs are characterized as densely packed aggregates of vesicular or tubular membranes of

337 variable form and size. In transverse sections, the TAs appear as a honeycomb-like structure displaying a para-
338 crystalline order (Fig. 10c&d, 11a). In longitudinal sections, the TAs run parallel to the sarcomeres (Fig. 10e&f,
339 11b). The TAs were either single-walled (Fig. 11c&d) or double-walled empty tubules (Fig. 11 e&f) and contain
340 mitophagy structure (Fig. 11c). Glycogen granules were occasionally found between the double-walled tubules
341 (Fig. 11e). Tubules in large aggregates show sub-clusters with different tubule orientation relative to the
342 sarcomere (Fig. 11a) either longitudinal, oblique or perpendicular within a single section (Fig. 11 a,b,&f).
343

Discussion

The secretory proprotein CgA is widely expressed in endocrine and neuroendocrine tissues as well as in the central nervous system, and is co-released with the resident hormones (Winkler and Fischer-Colbrie 1992; Montero-Hadjadje et al. 2008; Bartolomucci et al. 2011). Here, we detected CgA expression in GAS muscle and found that its absence, in *Chga*-KO mice, caused impaired muscle function. Based on the very low mRNA level yet strong protein expression it is possible that the source of processed CgA is from the axon terminals that innervate the muscle rather than the muscle cell itself. It has been reported that mRNA is transported from the cell body to the axon terminal where it is translated into protein and released exocytotically into the innervating tissue (Kar, et al. 2013; Jung, et al. 2014; Gervasi, et al. 2016). Hence the effects of CgA may well be paracrine in origin rather than autocrine. Secretogranin II, another member of the chromogranin/secretogranin protein family, has also been detected in hind limb muscle and cultured myotubes (Egger, et al. 2007). Supplementation with CgA in *Chga*-KO mice restored exercise ability. Together this data suggest a novel role for endogenous CgA in skeletal muscle function. It should be pointed out that the full-length CgA protein has recently been implicated in the regulation of myocardial contractility and angiogenesis (Crippa et al. 2013; Pasqua, et al. 2013). However, it remains to be established whether CgA activity in muscle function requires local processing to smaller bioactive fragments or not.

The signature defects that characterize the muscle phenotype in *Chga*-KO mice are (i) lack of exercise-induced stimulation of pAKT, pTBC1D1 and phospho-p38MAPK signaling, (ii) loss of GAS muscle mass, (iii) extensive formation of TA, (iv) disorganized cristae architecture in mitochondria, and (v) increased expression of *Tnfα* and *Ifnɣ*. We believe that the impaired maximum running speed and endurance in the treadmill exercise in *Chga*-KO mice are due to decreased in glucose uptake and glycolysis, and defects in glucose oxidation caused by defective mitochondria. In addition, the lack of adaptation to endurance exercise likely results from the impaired activation of stress responses, possibly resulting in deficiency in proliferation and differentiation of myogenic cells. It should be pointed out that *Chga*-KO mice are unique showing increased insulin sensitivity in the face of persistent hypertension (Mahapatra et al. 2005; Gayen et al. 2009; Biswas, et al. 2012; Bandyopadhyay, et al. 2015).

Decreased insulin-induced AKT phosphorylation at Ser473 and comparable phosphorylation of TBC1D1 at Thr590 confirm the muscle resistance phenotype that we have reported earlier (Gayen et al. 2009). Fibrosis is increasingly appreciated as a major contributor to metabolic dysregulation in obese humans and type 2 diabetics, and increased expression of collagen was observed in *Chga*-KO muscle, which may contribute to the insulin-resistant state (Sun, et al. 2013). Although AMPK signaling in response to exercise was normal in *Chga*-KO-GAS, it was ineffective at activating TBC1D1 signaling, which correlated with the reduced the ability of exercise to stimulate glucose uptake. Activation of p38 MAPK during muscle contraction can stimulate expression of *Pgc1α*, *Atf2* and *Mef2* and mediate mitochondrial adaptation (Akimoto, et al. 2005) and the p38MAPKγ-PGC1α pathway is central to the adaptive response to tissue damage in muscle (Pogozelski, et al. 2009). So the lack of stimulation of p38MAPK by either insulin or exercise likely prevented the post-exercise adaptation to tissue damage in the *Chga*-KO mice.

The gene expression pattern in *Chga*-KO-GAS suggested that mice were attempting to compensate for the impaired muscle function due to the loss of CgA by increasing the proliferation and differentiation of *Myod* and *Pax3* positive progenitor cells (Relaix et al. 2006; Young and Wagers 2010; Filareto et al. 2015). But the damaged muscle also triggers an immune response and the increased expression of *Ifnγ* could inhibit myogenin, via the major histocompatibility complex class II transactivator CIITA, and MyoD activities and prevent differentiation (Londhe and Davie 2011; Villalta, et al. 2011). Furthermore, the increased expression of IL-6 may have negative effects on glucose uptake in muscle (Kim, et al. 2004).

Mitochondria are essential to muscle function as they allow the efficient oxidation of glucose for the generation of ATP for contraction. Although the cristae volume density and cristae area are comparable in mitochondria between WT and *Chga*-KO mice, the decrease in mitochondrial number, volume density and area point to decreased mitochondrial function. Indeed cytochrome c oxidase (CCO) activity is decreased in *Chga*-KO muscle. The CCO enzyme complex is found on the inner mitochondrial membrane and serves as the final electron acceptor in mitochondrial electron transport, and has been reported to increase after endurance exercise (Samelman, et al. 2000). Thus, decreased CCO activity in *Chga*-KO GAS muscle coupled with decreased endurance performance is consistent with reduced mitochondrial function (Samelman et al. 2000).

Although TAs were first described by Engel in 1964 as granular “crystal-like” inclusions in skeletal muscle (Engel 1964), the mechanisms underlying the formation of TAs and their functional significance for

muscle function has remained elusive (Schubert et al. 2007; Schiaffino 2012). Our findings indicate an inverse association between TAs and exercise performance. TA structures can be generated *in vitro* by hypoxia in extensor digitorum longus (EDL) muscle or by potassium cyanide (Schiaffino et al. 1977). The detection of ubiquitin and hsp72 in these structures (Martin, et al. 1991; Muchowski and Wacker 2005) (Luan, et al. 2009), has led to the suggestion that the formation of TAs in skeletal muscle is comparable to formation of protein aggregates in neurodegenerative diseases but in these diseases protein aggregation occurs due to misfolding of proteins (Balch, et al. 2008; Douglas and Dillin 2010). In case of TAs, it was suggested that membrane-bound misfolded proteins could potentially induce aggregation of SR membranes to which they are bound by cross-linking but experimental evidence is lacking (Schiaffino 2012). One of the major functions of CgA is to sort proteins to the regulated secretory pathway (Chanat, et al. 1991; Taupenot, et al. 2002; Bartolomucci et al. 2011). Although the role of CgA in sorting or folding of membrane proteins is yet to be established, one could speculate such a role based on the observed pH-dependent association of CgA with secretory vesicle membranes (Yoo 1993). Therefore, lack of CgA could cause misfolding of membrane proteins allowing formation of TAs.

In conclusion, CgA deficiency causes a myopathic signature in skeletal muscle displaying extensive formation of TA signifying SR reorganization into multiple longitudinally oriented tubules with SERCA in the membrane and calsequestrin in the lumen. This myopathy is also characterized by muscle energy deficiency and the inability to regenerate after exercise-induced tissue damage. The net result is impaired performance in treadmill exercise.

Acknowledgments

Transmission Electron Microscopy was conducted at the Cellular & Molecular Medicine Electron Microscopy Core Facility at UCSD. Mahata's personal fund and UCSD Academic Senate Grant (RO091B) supported this work. SM was supported by the Noland Scholarship from Caltech.

Declaration of interest

There is no conflict of interest that could be perceived as prejudicing the impartiality of the research reported.

References

Aardal S, Helle KB, Elsayed S, Reed RK & Serck-Hanssen G 1993 Vasostatins, comprising the N-terminal domain of chromogranin A, suppress tension in isolated human blood vessel segments. *J Neuroendocrinol* **5** 405-412.

Akimoto T, Pohnert SC, Li P, Zhang M, Gumbs C, Rosenberg PB, Williams RS & Yan Z 2005 Exercise stimulates Pgc-1alpha transcription in skeletal muscle through activation of the p38 MAPK pathway. *J Biol Chem* **280** 19587-19593.

Angelone T, Quintieri AM, Brar BK, Limchaiyawat PT, Tota B, Mahata SK & Cerra MC 2008 The antihypertensive chromogranin a peptide catestatin acts as a novel endocrine/paracrine modulator of cardiac inotropism and lusitropism. *Endocrinology* **149** 4780-4793.

Armstrong RB, Warren GL & Warren JA 1991 Mechanisms of exercise-induced muscle fibre injury. *Sports Med* **12** 184-207.

Aronson D, Violan MA, Dufresne SD, Zangen D, Fielding RA & Goodyear LJ 1997 Exercise stimulates the mitogen-activated protein kinase pathway in human skeletal muscle. *J Clin Invest* **99** 1251-1257.

Balch WE, Morimoto RI, Dillin A & Kelly JW 2008 Adapting proteostasis for disease intervention. *Science* **319** 916-919.

Bandyopadhyay GK, Lu M, Avolio E, Siddiqui JA, Gayen JR, Wollam J, Vu CU, Chi NW, O'Connor DT & Mahata SK 2015 Pancreastatin-dependent inflammatory signaling mediates obesity-induced insulin resistance. *Diabetes* **64** 104-116.

Banks P, Helle KB & Mayor D 1969 Evidence for the presence of a chromogranin-like protein in bovine splenic nerve granules. *Mol Pharmacol* **5** 210-212.

Bartlett SF, Lagercrantz H & Smith AD 1976 Gel electrophoresis of soluble and insoluble proteins of noradrenergic vesicles from ox splenic nerve: a comparison with proteins of adrenal chromaffin granules. *Neuroscience* **1** 339-344.

Bartolomucci A, Possenti R, Mahata SK, Fischer-Colbrie R, Loh YP & Salton SR 2011 The extended granin family: structure, function, and biomedical implications. *Endocr Rev* **32** 755-797.

Bertorini TE, Brumback RA, Kula RW & Engel WK 1977 Electrophysiologic and histochemical observations in five patients with muscle phosphorylase deficiency (MPD). *Trans Am Neurol Assoc* **102** 141-142.

Biswas N, Gayen J, Mahata M, Su Y, Mahata SK & O'Connor DT 2012 Novel peptide isomer strategy for stable inhibition of catecholamine release: application to hypertension. *Hypertension* **60** 1552-1559.

Boncompagni S, Protasi F & Franzini-Armstrong C 2012 Sequential stages in the age-dependent gradual formation and accumulation of tubular aggregates in fast twitch muscle fibers: SERCA and calsequestrin involvement. *Age (Dordr)* **34** 27-41.

Brumback RA, Staton RD & Susag ME 1981 Exercise-induced pain, stiffness, and tubular aggregation in skeletal muscle. *J Neurol Neurosurg Psychiatry* **44** 250-254.

Brumback RA, Susag ME & Gerst JW 1980 Animal model of human disease: defective skeletal muscle glucose and/or glycogen metabolism. *Am J Pathol* **101** 241-244.

Chanat E, Pimplikar SW, Stinchcombe JC & Huttner WB 1991 What the granins tell us about the formation of secretory granules in neuroendocrine cells. *Cell Biophys* **19** 85-91.

Colombo B, Curnis F, Foglieni C, Monno A, Arrigoni G & Corti A 2002 Chromogranin A expression in neoplastic cells affects tumor growth and morphogenesis in mouse models. *Cancer Res* **62** 941-946.

Conboy IM & Rando TA 2002 The regulation of Notch signaling controls satellite cell activation and cell fate determination in postnatal myogenesis. *Dev Cell* **3** 397-409.

Cornelio F & Di Donato S 1985 Myopathies due to enzyme deficiencies. *J Neurol* **232** 329-340.

Craig ID & Allen IV 1980 Tubular aggregates in murine dystrophy heterozygotes. *Muscle Nerve* **3** 134-140.

Crippa L, Bianco M, Colombo B, Gasparri AM, Ferrero E, Loh YP, Curnis F & Corti A 2013 A new chromogranin A-dependent angiogenic switch activated by thrombin. *Blood* **121** 392-402.

Crosson SM, Khan A, Printen J, Pessin JE & Saltiel AR 2003 PTG gene deletion causes impaired glycogen synthesis and developmental insulin resistance. *J Clin Invest* **111** 1423-1432.

De Potter WP, De Schaepdryver AF & Smith AD 1970a Release of chromogranin A and dopamine-beta-hydroxylase from adrenergic nerves during nerve stimulation. *Acta Physiol Scand* 8.

De Potter WP, Smith AD & De Schaepdryver AF 1970b Subcellular fractionation of splenic nerve: ATP, chromogranin A and dopamine beta-hydroxylase in noradrenergic vesicles. *Tissue Cell* **2** 529-546.

Douen AG, Ramlal T, Klip A, Young DA, Cartee GD & Holloszy JO 1989 Exercise-induced increase in glucose transporters in plasma membranes of rat skeletal muscle. *Endocrinology* **124** 449-454.

Douglas PM & Dillin A 2010 Protein homeostasis and aging in neurodegeneration. *J Cell Biol* **190** 719-729.

Duguez S, Feasson L, Denis C & Freyssenet D 2002 Mitochondrial biogenesis during skeletal muscle regeneration. *Am J Physiol Endocrinol Metab* **282** E802-809.

Egger M, Schgoer W, Beer AG, Jeschke J, Leierer J, Theurl M, Frauscher S, Tepper OM, Niederwanger A, Ritsch A, et al. 2007 Hypoxia up-regulates the angiogenic cytokine secretoneurin via an HIF-1alpha- and basic FGF-dependent pathway in muscle cells. *FASEB J* **21** 2906-2917.

Engel WK 1964 Mitochondrial Aggregates in Muscle Disease. *J Histochem Cytochem* **12** 46-48.

Filareto A, Rinaldi F, Arpke RW, Darabi R, Belanto JJ, Toso EA, Miller AZ, Ervasti JM, McIvor RS, Kyba M, et al. 2015 Pax3-induced expansion enables the genetic correction of dystrophic satellite cells. *Skelet Muscle* **5** 36.

Friden J, Lieber RL & Thornell LE 1991 Subtle indications of muscle damage following eccentric contractions. *Acta Physiol Scand* **142** 523-524.

Gayen JR, Saberi M, Schenk S, Biswas N, Vaingankar SM, Cheung WW, Najjar SM, O'Connor DT, Bandyopadhyay G & Mahata SK 2009 A novel pathway of insulin sensitivity in chromogranin a null mice: A crucial role for pancreastatin in glucose homeostasis. *J Biol Chem* **284** 28498-28509.

Gervasi NM, Scott SS, Aschrafi A, Gale J, Vohra SN, MacGibeny MA, Kar AN, Gioio AE & Kaplan BB 2016 The local expression and trafficking of tyrosine hydroxylase mRNA in the axons of sympathetic neurons. *RNA* **22** 883-895.

Gibala M 2009 Molecular responses to high-intensity interval exercise. *Appl Physiol Nutr Metab* **34** 428-432.

Goodyear LJ, Chang PY, Sherwood DJ, Dufresne SD & Moller DE 1996 Effects of exercise and insulin on mitogen-activated protein kinase signaling pathways in rat skeletal muscle. *Am J Physiol* **271** E403-408.

Goodyear LJ, Hirshman MF & Horton ES 1991a Exercise-induced translocation of skeletal muscle glucose transporters. *Am J Physiol* **261** E795-799.

Goodyear LJ, Hirshman MF, Smith RJ & Horton ES 1991b Glucose transporter number, activity, and isoform content in plasma membranes of red and white skeletal muscle. *Am J Physiol* **261** E556-561.

Goodyear LJ & Kahn BB 1998 Exercise, glucose transport, and insulin sensitivity. *Annu Rev Med* **49** 235-261.

Goodyear LJ, King PA, Hirshman MF, Thompson CM, Horton ED & Horton ES 1990 Contractile activity increases plasma membrane glucose transporters in absence of insulin. *Am J Physiol* **258** E667-672.

Helle KB 1966 Some chemical and physical properties of the soluble protein fraction of bovine adrenal chromaffin granules. *Mol Pharmacol* **2** 298-310.

Hirshman MF, Goodyear LJ, Wardzala LJ, Horton ED & Horton ES 1990 Identification of an intracellular pool of glucose transporters from basal and insulin-stimulated rat skeletal muscle. *J Biol Chem* **265** 987-991.

Jung H, Gkogkas CG, Sonenberg N & Holt CE 2014 Remote control of gene function by local translation. *Cell* **157** 26-40.

Kar AN, MacGibeny MA, Gervasi NM, Gioio AE & Kaplan BB 2013 Intra-axonal synthesis of eukaryotic translation initiation factors regulates local protein synthesis and axon growth in rat sympathetic neurons. *J Neurosci* **33** 7165-7174.

Kim HJ, Higashimori T, Park SY, Choi H, Dong J, Kim YJ, Noh HL, Cho YR, Cline G, Kim YB, et al. 2004 Differential effects of interleukin-6 and -10 on skeletal muscle and liver insulin action in vivo. *Diabetes* **53** 1060-1067.

Korenyi-Both A, Smith BH & Baruah JK 1977 McArdle's syndrome. Fine structural changes in muscle. *Acta Neuropathol* **40** 11-19.

Lauritzen HP, Galbo H, Toyoda T & Goodyear LJ 2010 Kinetics of contraction-induced GLUT4 translocation in skeletal muscle fibers from living mice. *Diabetes* **59** 2134-2144.

Layzer RB, Rowland LP & Ranney HM 1967 Muscle phosphofructokinase deficiency. *Arch Neurol* **17** 512-523.

Londhe P & Davie JK 2011 Gamma interferon modulates myogenesis through the major histocompatibility complex class II transactivator, CIITA. *Mol Cell Biol* **31** 2854-2866.

Luan X, Chen B, Liu Y, Zheng R, Zhang W & Yuan Y 2009 Tubular aggregates in paralysis periodica paramyotonica with T704M mutation of SCN4A. *Neuropathology* **29** 579-584.

Machida S & Booth FW 2004 Insulin-like growth factor 1 and muscle growth: implication for satellite cell proliferation. *Proc Nutr Soc* **63** 337-340.

Mahapatra NR, O'Connor DT, Vaingankar SM, Hikim AP, Mahata M, Ray S, Staite E, Wu H, Gu Y, Dalton N, et al. 2005 Hypertension from targeted ablation of chromogranin A can be rescued by the human ortholog. *J Clin Invest* **115** 1942-1952.

538 Mahata SK, Mahapatra NR, Mahata M, Wang TC, Kennedy BP, Ziegler MG & O'Connor DT 2003
539 Catecholamine secretory vesicle stimulus-transcription coupling in vivo. Demonstration by a novel transgenic
540 promoter/photoprotein reporter and inhibition of secretion and transcription by the chromogranin A fragment
541 catestatin. *J Biol Chem* **278** 32058-32067.
542 Mahata SK, O'Connor DT, Mahata M, Yoo SH, Taupenot L, Wu H, Gill BM & Parmer RJ 1997 Novel autocrine
543 feedback control of catecholamine release. A discrete chromogranin A fragment is a noncompetitive nicotinic
544 cholinergic antagonist. *J Clin Invest* **100** 1623-1633.
545 Martin JE, Mather K, Swash M & Gray AB 1991 Expression of heat shock protein epitopes in tubular
546 aggregates. *Muscle Nerve* **14** 219-225.
547 Middelbeek RJ, Chambers MA, Tantiwong P, Treebak JT, An D, Hirshman MF, Musi N & Goodyear LJ 2013
548 Insulin stimulation regulates AS160 and TBC1D1 phosphorylation sites in human skeletal muscle. *Nutr Diabetes*
549 **3** e74.
550 Montero-Hadjadje M, Vaingankar S, Elias S, Tostivint H, Mahata SK & Anouar Y 2008 Chromogranins A and B
551 and secretogranin II: evolutionary and functional aspects. *Acta Physiol (Oxf)* **192** 309-324.
552 Muchowski PJ & Wacker JL 2005 Modulation of neurodegeneration by molecular chaperones. *Nat Rev Neurosci*
553 **6** 11-22.
554 Osman AA, Pendergrass M, Koval J, Maezono K, Cusi K, Pratipanawatr T & Mandarino LJ 2000 Regulation of
555 MAP kinase pathway activity in vivo in human skeletal muscle. *Am J Physiol Endocrinol Metab* **278** E992-999.
556 Pasqua T, Corti A, Gentile S, Pochini L, Bianco M, Metz-Boutigue MH, Cerra MC, Tota B & Angelone T 2013
557 Full-length human chromogranin-A cardioactivity: myocardial, coronary, and stimulus-induced processing
558 evidence in normotensive and hypertensive male rat hearts. *Endocrinology* **154** 3353-3365.
559 Pasqua T, Mahata S, Bandyopadhyay GK, Biswas A, Perkins GA, Sinha Hikim AP, Goldstein DS, Eiden LE &
560 Mahata SK 2016 Impact of Chromogranin A deficiency on catecholamine storage, catecholamine granule
561 morphology, and chromaffin cell energy metabolism in vivo. *Cell Tissue Res* **363** 693-712.
562 Paulsen G, Egner I, Raastad T, Reinholt F, Owe S, Lauritzen F, Brorson SH & Koskinen S 2013 Inflammatory
563 markers CD11b, CD16, CD66b, CD68, myeloperoxidase and neutrophil elastase in eccentric exercised human
564 skeletal muscles. *Histochem Cell Biol* **139** 691-715.
565 Perrey S & Rupp T 2009 Altitude-induced changes in muscle contractile properties. *High Alt Med Biol* **10** 175-
566 182.
567 Pogozelski AR, Geng T, Li P, Yin X, Lira VA, Zhang M, Chi JT & Yan Z 2009 p38gamma mitogen-activated
568 protein kinase is a key regulator in skeletal muscle metabolic adaptation in mice. *PLoS One* **4** e7934.
569 Ratti S, Curnis F, Longhi R, Colombo B, Gasparri A, Magni F, Manera E, Metz-Boutigue MH & Corti A 2000
570 Structure-activity relationships of chromogranin A in cell adhesion. Identification of an adhesion site for
571 fibroblasts and smooth muscle cells. *J Biol Chem* **275** 29257-29263.
572 Relaix F, Montarras D, Zaffran S, Gayraud-Morel B, Rocancourt D, Tajbakhsh S, Mansouri A, Cumano A &
573 Buckingham M 2006 Pax3 and Pax7 have distinct and overlapping functions in adult muscle progenitor cells. *J*
574 *Cell Biol* **172** 91-102.

575 Richter EA & Ruderman NB 2009 AMPK and the biochemistry of exercise: implications for human health and
576 disease. *Biochem J* **418** 261-275.
577 Sakamoto K, Aschenbach WG, Hirshman MF & Goodyear LJ 2003 Akt signaling in skeletal muscle: regulation
578 by exercise and passive stretch. *Am J Physiol Endocrinol Metab* **285** E1081-1088.
579 Sakamoto K & Holman GD 2008 Emerging role for AS160/TBC1D4 and TBC1D1 in the regulation of GLUT4
580 traffic. *Am J Physiol Endocrinol Metab* **295** E29-37.
581 Samelman TR, Shiry LJ & Cameron DF 2000 Endurance training increases the expression of mitochondrial and
582 nuclear encoded cytochrome c oxidase subunits and heat shock proteins in rat skeletal muscle. *Eur J Appl*
583 *Physiol* **83** 22-27.
584 Sanchez-Margalet V, Gonzalez-Yanes C, Najib S & Santos-Alvarez J 2010 Metabolic effects and mechanism of
585 action of the chromogranin A-derived peptide pancreastatin. *Regul Pept* **161** 8-14.
586 Schiaffino S 2012 Tubular aggregates in skeletal muscle: just a special type of protein aggregates?
587 *Neuromuscul Disord* **22** 199-207.
588 Schiaffino S & Mammucari C 2011 Regulation of skeletal muscle growth by the IGF1-Akt/PKB pathway: insights
589 from genetic models. *Skelet Muscle* **1** 4.
590 Schiaffino S, Severin E, Cantini M & Sartore S 1977 Tubular aggregates induced by anoxia in isolated rat
591 skeletal muscle. *Lab Invest* **37** 223-228.
592 Schubert W, Sotgia F, Cohen AW, Capozza F, Bonuccelli G, Bruno C, Minetti C, Bonilla E, Dimauro S & Lisanti
593 MP 2007 Caveolin-1(-/-)- and caveolin-2(-/-)-deficient mice both display numerous skeletal muscle
594 abnormalities, with tubular aggregate formation. *Am J Pathol* **170** 316-333.
595 Smith AD & Winkler H 1967 Purification and properties of an acidic protein from chromaffin granules of bovine
596 adrenal medulla. *Biochem J* **103** 483-492.
597 Smith WJ & Kirshner N 1967 A specific soluble protein from the catecholamine storage vesicles of bovine
598 adrenal medulla. I. Purification and chemical characterization. *Mol Pharmacol* **3** 52-62.
599 Somogyi P, Hodgson AJ, DePotter RW, Fischer-Colbrie R, Schober M, Winkler H & Chubb IW 1984
600 Chromogranin immunoreactivity in the central nervous system. Immunochemical characterisation, distribution
601 and relationship to catecholamine and enkephalin pathways. *Brain Res* **320** 193-230.
602 Somwar R, Perreault M, Kapur S, Taha C, Sweeney G, Ramlal T, Kim DY, Keen J, Cote CH, Klip A, et al. 2000
603 Activation of p38 mitogen-activated protein kinase alpha and beta by insulin and contraction in rat skeletal
604 muscle: potential role in the stimulation of glucose transport. *Diabetes* **49** 1794-1800.
605 Sun K, Tordjman J, Clement K & Scherer PE 2013 Fibrosis and adipose tissue dysfunction. *Cell Metab* **18** 470-
606 477.
607 Tarui S, Okuno G, Ikura Y, Tanaka T, Suda M & Nishikawa M 1965 Phosphofructokinase Deficiency in Skeletal
608 Muscle. A New Type of Glycogenosis. *Biochem Biophys Res Commun* **19** 517-523.
609 Tatemoto K, Efendic S, Mutt V, Makk G, Feistner GJ & Barchas JD 1986 Pancreastatin, a novel pancreatic
610 peptide that inhibits insulin secretion. *Nature* **324** 476-478.

Taupenot L, Harper KL, Mahapatra NR, Parmer RJ, Mahata SK & O'Connor DT 2002 Identification of a novel sorting determinant for the regulated pathway in the secretory protein chromogranin A. *J Cell Sci* **115** 4827-4841.

Tota B, Angelone T, Mazza R & Cerra MC 2008 The chromogranin A-derived vasostatins: new players in the endocrine heart. *Curr Med Chem* **15** 1444-1451.

Tota B, Gentile S, Pasqua T, Bassino E, Koshimizu H, Cawley NX, Cerra MC, Loh YP & Angelone T 2012 The novel chromogranin A-derived serpinin and pyroglutaminated serpinin peptides are positive cardiac beta-adrenergic-like inotropes. *FASEB journal : official publication of the Federation of American Societies for Experimental Biology* **26** 2888-2898.

Vichaiwong K, Purohit S, An D, Toyoda T, Jessen N, Hirshman MF & Goodyear LJ 2010 Contraction regulates site-specific phosphorylation of TBC1D1 in skeletal muscle. *Biochem J* **431** 311-320.

Villalta SA, Deng B, Rinaldi C, Wehling-Henricks M & Tidball JG 2011 IFN-gamma promotes muscle damage in the mdx mouse model of Duchenne muscular dystrophy by suppressing M2 macrophage activation and inhibiting muscle cell proliferation. *J Immunol* **187** 5419-5428.

Volknandt W, Schober M, Fischer-Colbrie R, Zimmermann H & Winkler H 1987 Cholinergic nerve terminals in the rat diaphragm are chromogranin A immunoreactive. *Neurosci Lett* **81** 241-244.

Wagers AJ & Conboy IM 2005 Cellular and molecular signatures of muscle regeneration: current concepts and controversies in adult myogenesis. *Cell* **122** 659-667.

Winkler H & Fischer-Colbrie R 1992 The chromogranins A and B: the first 25 years and future perspectives. *Neuroscience* **49** 497-528.

Yoo SH 1993 pH-dependent association of chromogranin A with secretory vesicle membrane and a putative membrane binding region of chromogranin A. *Biochemistry* **32** 8213-8219.

Young AP & Wagers AJ 2010 Pax3 induces differentiation of juvenile skeletal muscle stem cells without transcriptional upregulation of canonical myogenic regulatory factors. *J Cell Sci* **123** 2632-2639.

Legends to the Figures.

Figure 1. Impaired endurance capacity in *Chga*-KO mice. (a) Increased body weight in *Chga*-KO mice. (b) GAS muscle weight is decreased in *Chga*-KO mice. (c) The V_{O2} maximal speed in an incremental treadmill running test in WT and *Chga*-KO mice. (d) Endurance exercise capacity was evaluated by the time to reach exhaustion when mice were run at 60% of the average V_{O2} maximal speed. **Supplementation of *Chga*-KO mice with CgA for 15 days restored endurance capacity.** (e) Maximal speed. (f) Endurance exercise capacity. **Expressions of CgA/*Chga* in GAS muscle**. (g&h) Western blot showing expression of CgA GAS muscle in WT mice and no expression in *Chga*-KO (KO) mice. (i) Expression of *Chga* in WT and *Chga*-KO mice. Expressions of *Chga*, *Chgb*, and *Scg2* genes in GAS muscle (j), adrenal gland (k), pituitary gland (l), hypothalamus (m), and pancreatic islets (n).

Figure 2. Assessment of insulin-induced signaling by Western blot in GAS muscle. Mice were treated with saline or insulin (0.4 mU/g BW) for 10 minutes before tissue harvesting. (a) Western blots showing expression of phospho-AKT at Ser473, total AKT, phospho-TBC1D1 at Thr590, total PBC1D1, phospho-P38 at Thr180/Tyr182, and total P38 in WT and *Chga*-KO mice. Densitometric values showing pS473-AKT/total AKT (b), pT590-TBC1D1/total TBC1D1 (c), and pT180/Y182-P38/total P38 in WT and *Chga*-KO mice after endurance exercise. Note compromised insulin-induced signaling in *Chga*-KO mice.

Figure 3. Evaluation of exercise-induced signaling by Western blot in WT and *Chga*-KO GAS muscle. Mice were treated with saline or insulin (0.4 mU/g BW) for 10 minutes before tissue harvesting. Western blots showing expression of phospho-AKT at Ser473, total AKT, AMPKα at Thr172, total AMPK, phospho-TBC1D1 at Thr590, phospho-TBC1D1 at Ser700, total PBC1D1, phospho-P38 at Thr180/Tyr182, and total P38 in WT and KO mice. Densitometric values showing pS473-AKT/AKT (b), pT172-AMPK□/AMPK (c), pT590-TBC1D1/TBC1D1 (d), pS700-TBC1D1/TBC1D1 (e), and pT180/Y182-P38/P38 (f). Note compromised exercise-induced signaling in *Chga*-KO mice.

Figure 4. Substrate uptake and metabolism in sedentary and exercised WT and *Chga*-KO GAS muscle. (a) Blood glucose. (b) 2-deoxy glucose (2DG) uptake. (c) *Glut4* mRNA level. (d) Plasma triglyceride (TG). (e) Utilization of glucose-6-phosphate (G6P). Note low G6P content is an indication of increased G6P utilization. (f) Fatty acid (palmitic acid) uptake. (g) Expression of *Cd36* gene. (h) Fatty acid oxidation (as evaluated by the amount of acid soluble metabolites). Note low values indicate decreased fatty acid oxidation.

Figure 5. Gene expression in sedentary WT and *Chga*-KO mice. (a) Relative mRNA levels of myogenin (*Myog*), myogenic differentiation antigen (*MyoD*), nestin (*Nes*), myogenic factor 5 (*Myf5*), paired box gene 3 (*Pax3*), paired box gene 7 (*Pax7*), and vascular endothelial growth factor (*Vegf*) genes. (b) Relative mRNA levels of F-box only protein 32(*Fboxo32*/ *Atrogin1*), ring finger protein 28 (*Trim63*/*Murf1*), tumor necrosis factor alpha (*Tnfα*), interferon, gamma (*Ifnγ*), interleukin 6 (*Il6*), interleukin 1 beta (*I1β*□□□□□□□interleukin 10 (*Il10*) genes. Statistical analyses were made by multiple *t* tests using Holm-Sidak's correction method.

Figure 6. Increased fibrosis in GAS muscle of sedentary mice. (a&b) Hematoxylin and eosin-stained transverse sections of GAS muscle in sedentary WT and *Chga*-KO mice. The arrows show dot-like irregular structures in the myofibrillar region. Expression of fibrotic genes: Collagen type I alpha 1 (*Col1a1*) (c&d), collagen type III alpha 1 (*Col3a1*) (c&e), Lysyl oxidase (*Lox*) (c&f), fibronectin 1 (*Fn1*) (c&g), and smooth muscle aortic alpha-actin (*Acta2)* (c&h). **Transmission electron microscope (TEM) micrographs showing accumulation of collagen:** Low magnification (2900x) photographs in WT and *Chga*-KO GAS muscle (i&j). High magnification (23,000x) photographs showing collagen in *Chga*-KO muscle (k). COL, collagen; GLY, glycogen; SSM, subsarcolemmal mitochondria; TT, T-tubule.

Fig. 7. TEM micrographs in GAS muscle of sedentary mice. Intermyofibrillar (IMF) mitochondria at magnification 2500x (a), 15,000x (b), and 30,000x in WT mice. Note the triad comprising of T-tubule (shown by black arrow) flanked by smooth sarcoplasmic reticulum (shown by red arrow). IMF mitochondria at magnification 2500x (d), 15,000x (e), and 30,000x (f) in *Chga*-KO mice. Note glycogen (GLY) granules either in one or both sides of the Z-disc and smaller triad in *Chga*-KO mice. **Morphometric analyses (15 mitochondria from 15 sections per mouse for a total of 4 mice) of TEM micrographs from sedentary WT and *Chga*-KO mice.** (g) Mitochondrial volume density (%). (h) Mitochondrial area (nm^2). (i) Cristae volume density (%). (j) Cristae area (nm^2). (k) Cytochrome C oxidase (CCO) activity in sedentary WT and *Chga*-KO mice.

Fig. 8. Subsarcolemmal mitochondria (SSM) in sedentary WT and *Chga*-KO GAS muscle. SSM and IMF mitochondria at magnification 2500x in WT mice. (b) SSM at magnification 30,000x in WT mice. Note cristae emerging from the inner mitochondrial membrane. (c) SSM and IMF mitochondria at magnification 2500x in *Chga*-KO mice. Note inclusion body in the subsarcolemmal region. (d) SSM at magnification 30,000x in *Chga*-KO mice. Note mitophagy (MPG), fewer cristae and glycogen granules (GLY).

Fig. 9. Mitochondria and TA in exercised longitudinally sectioned WT and *Chga*-KO GAS muscle. (a) IMF mitochondria at 2500x in WT mice. (b) TA at 2500x in *Chga*-KO mice. (c) SSM at 30,000x with dilated cristae and long cristae in WT mice. (d) SSM at 30,000x with round, oval and smaller cristae in *Chga*-KO mice. (e) IMF mitochondria at 30,000x with dilated cristae and T-tubule in WT mice. (f) IMF mitochondria at 30,000x with dilated cristae and normal triad. Black arrow points to T-tubule and red arrow points to smooth sarcoplasmic reticulum.

Fig. 10. Tubular aggregates (TAs) in sedentary *Chga*-KO GAS muscle. (a&b) Transverse sections showing SSM and IFM and the absence of TA in subsarcolemmal and myofibrillar regions. Note elongated IFM. **TAs in transverse sections.** TA in subsarcolemmal (c) and myofibrillar (d) regions. **TAs in longitudinal sections.** TA in subsarcolemmal (e) and myofibrillar (f) regions. Arrow points to sarcolemma.

Fig. 11. Tubular aggregates (TAs) in sedentary *Chga*-KO GAS muscle. (a) Transverse section showing a large aggregate where sub-clusters display different tubule orientation

relative to the sarcomere and mitochondria (MITO) in the outer border of TA. The inset shows a honeycomb-like TA. (b) Longitudinal section showing a TA, which runs parallel to the sarcomere. (c) Longitudinal section showing a TA with paracrystalline single-walled tubules of comparable area and a damaged mitochondrion (mitophagy). (d) Longitudinal section showing a TA, where paracrystalline tubules are of different areas. (e) Longitudinal section showing a TA with double-walled tubules and glycogen (GLY) granules in between two tubules. (f) Longitudinal section showing a TA where tubules are cut in the longitudinal, oblique or perpendicular to the sarcomere. Note triad and glycogen granules in the vicinity of TA. Black arrow points to T-tubule and red arrow points to smooth sarcoplasmic reticulum.

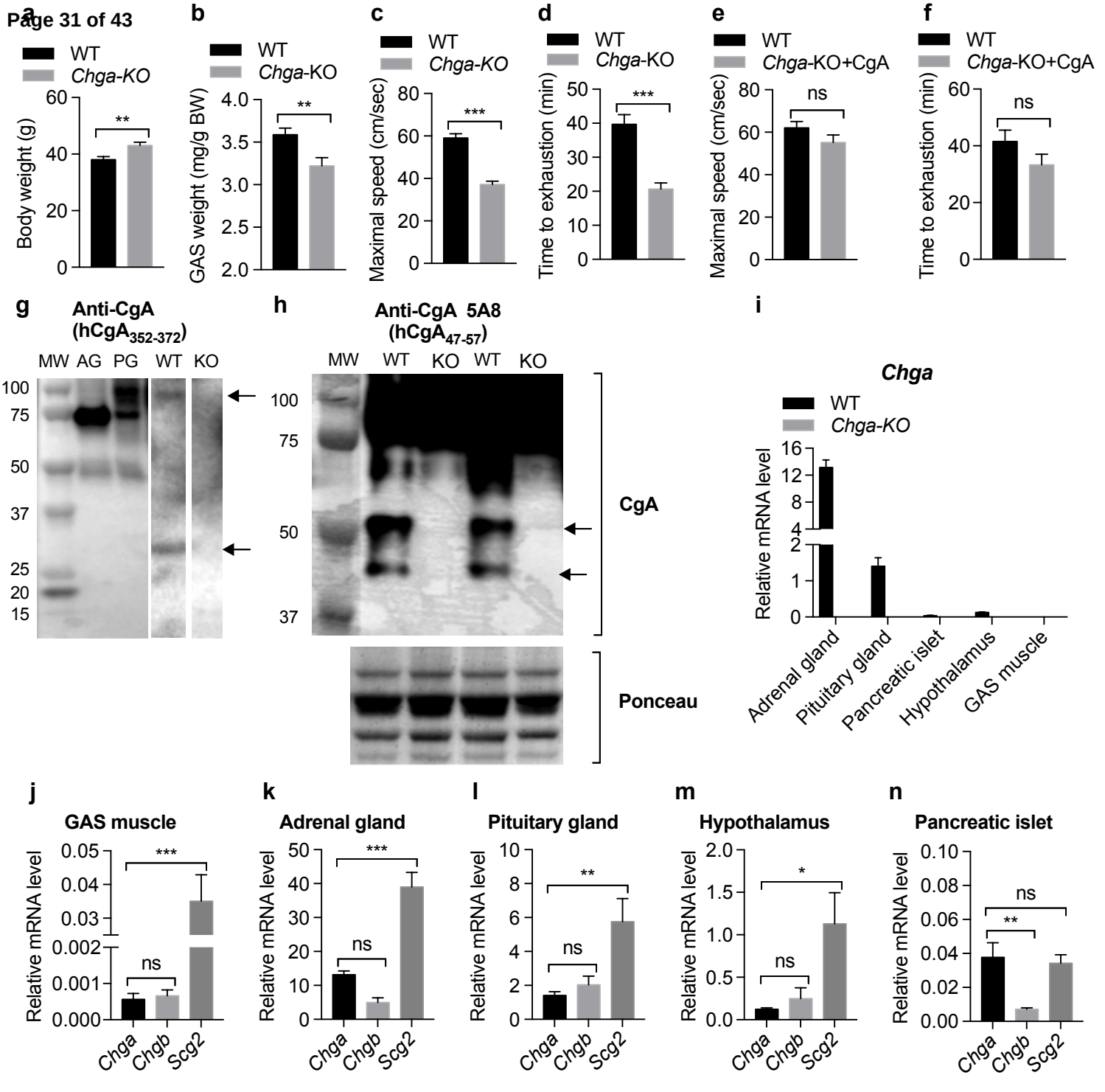
a
WT
Chga-KO
Body weight (g)
60
40
20
0
**
b
WT
Chga-KO
GAS weight (mg/g BW)
4.0
3.5
3.0
2.5
2.0
**
c
WT
Chga-KO
Maximal speed (cm/sec)
80
60
40
20
0
***
d
WT
Chga-KO
Time to exhaustion (min)
50
40
30
20
10
0
***
e
WT
Chga-KO+CgA
Maximal speed (cm/sec)
80
60
40
20
0
ns
f
WT
Chga-KO+CgA
Time to exhaustion (min)
60
40
20
0
ns
g
Anti-CgA
(hCgA352-372)
MW AG PG WT KO
100
75
50
37
25
20
15
h
Anti-CgA 5A8
(hCgA47-57)
MW WT KO WT KO
100
75
50
37
CgA
Ponceau
i
Chga
WT
Chga-KO
Relative mRNA level
16
12
8
4
2
1
0
Adrenal gland
Pituitary gland
Pancreatic islet
Hypothalamus
GAS muscle
j
GAS muscle
Relative mRNA level
0.05
0.04
0.03
0.002
0.001
0.000
***
ns
Chga
Chgb
Scg2
k
Adrenal gland
Relative mRNA level
50
40
30
20
10
0
***
ns
Chga
Chgb
Scg2
l
Pituitary gland
Relative mRNA level
10
8
6
4
2
0
**
ns
Chga
Chgb
Scg2
m
Hypothalamus
Relative mRNA level
2.0
1.5
1.0
0.5
0.0
*
ns
Chga
Chgb
Scg2
n
Pancreatic islet
Relative mRNA level
0.10
0.08
0.06
0.04
0.02
0.00
ns
**
Chga
Chgb
Scg2

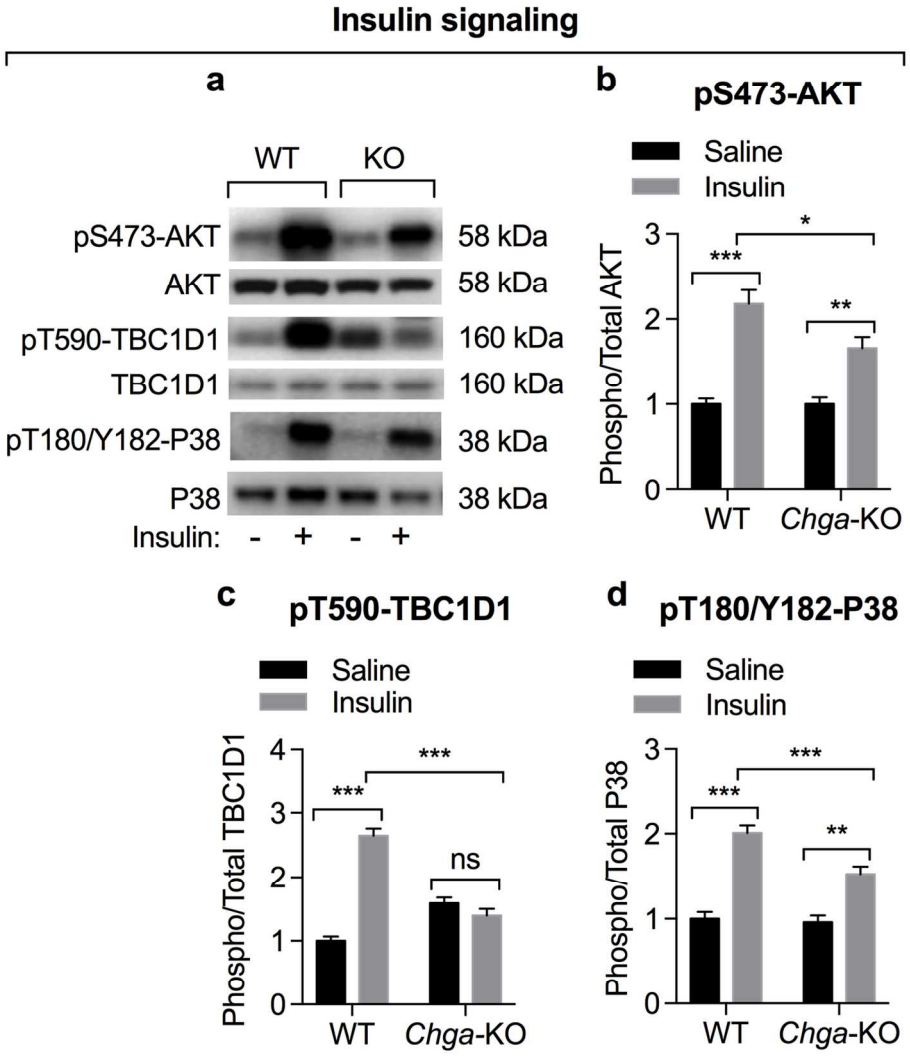

130x143mm (300 x 300 DPI)

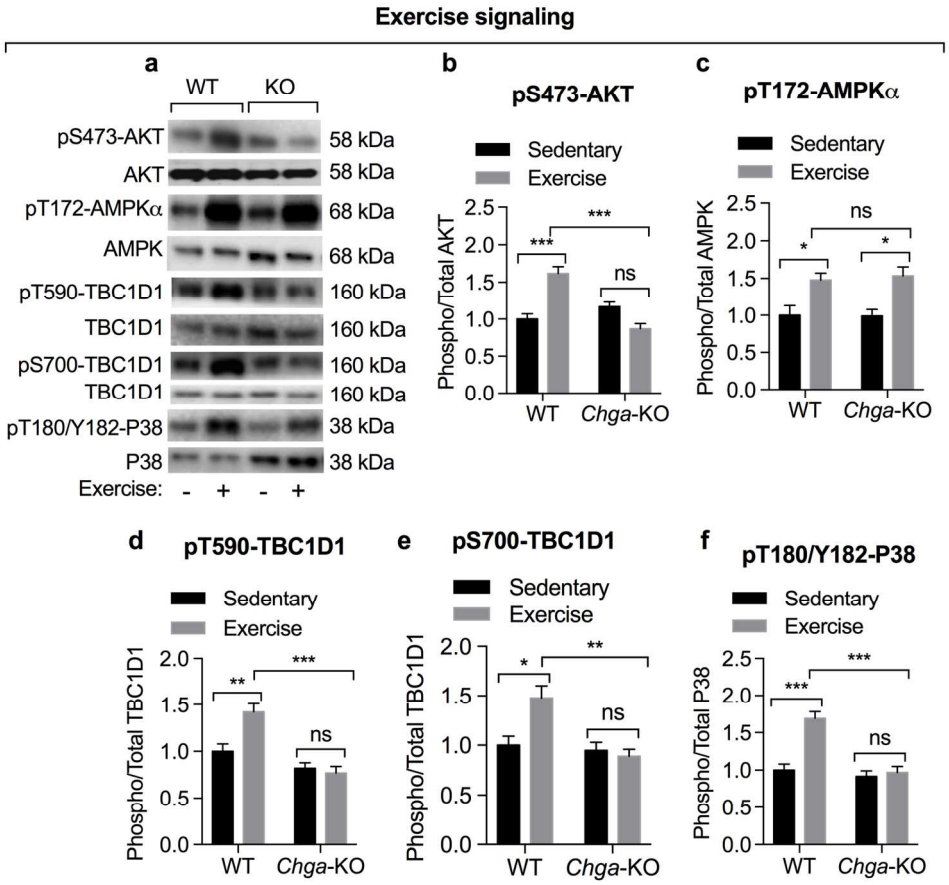

149x136mm (300 x 300 DPI)

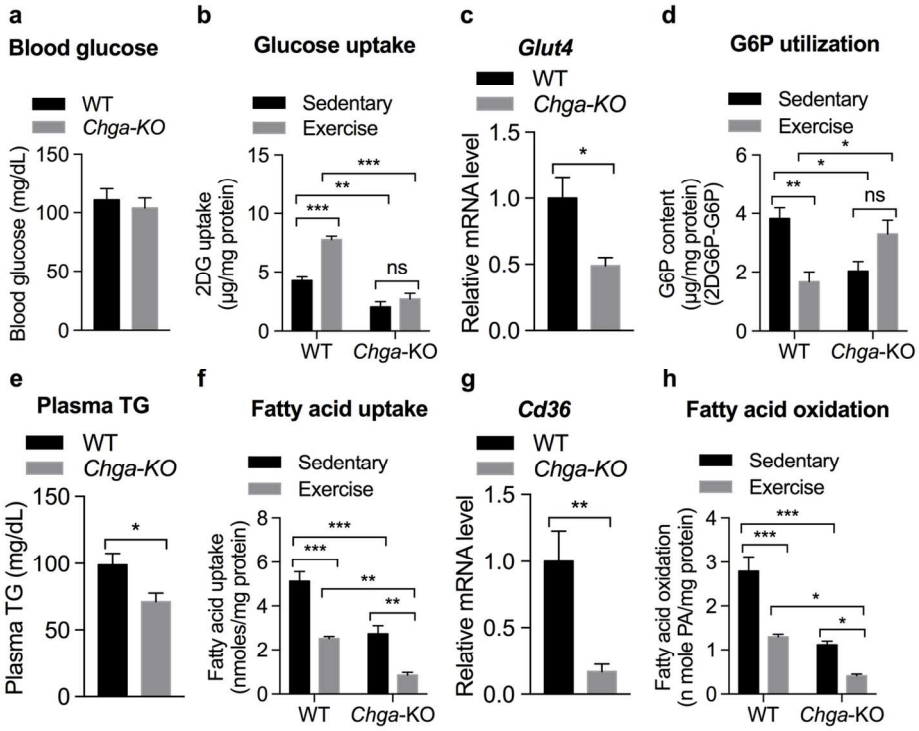

130x98mm (300 x 300 DPI)

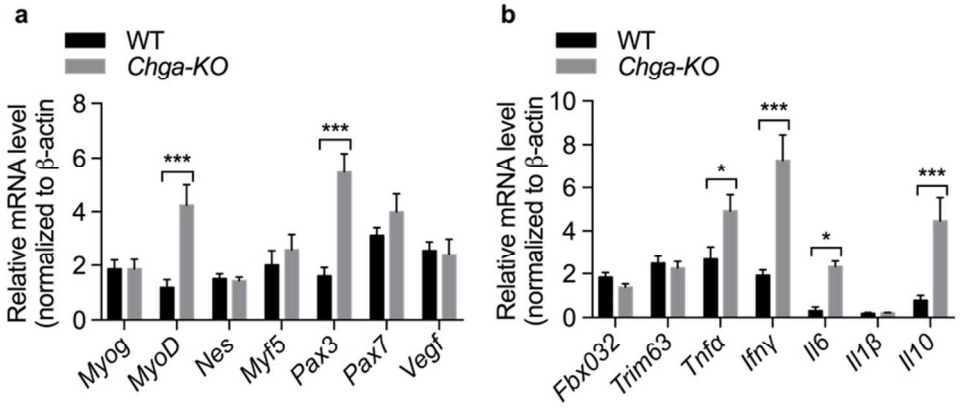

74x33mm (300 x 300 DPI)

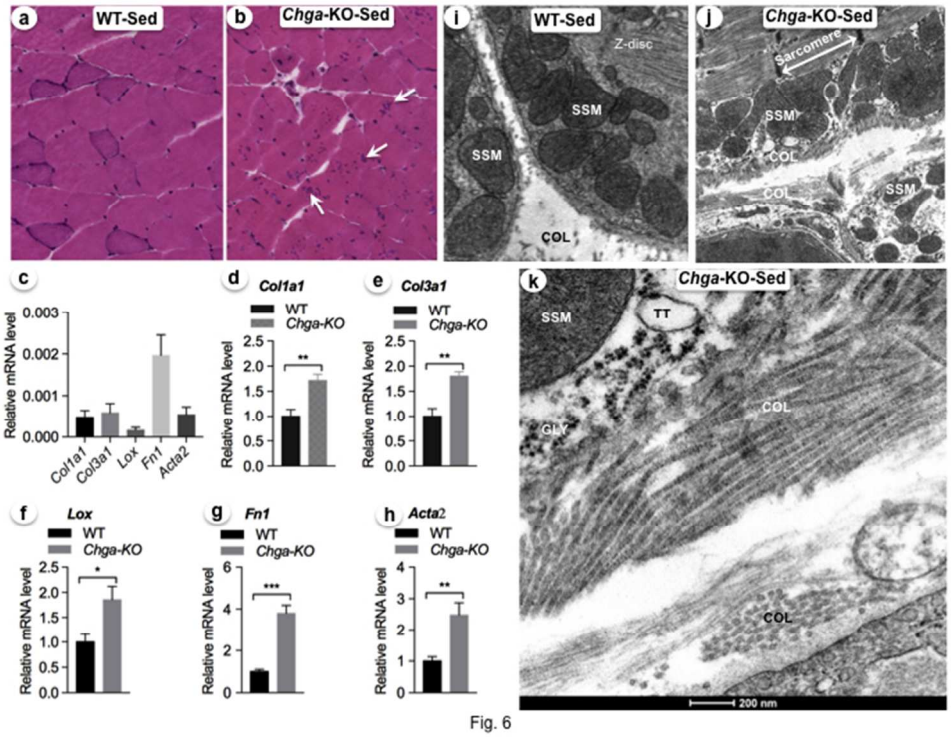

Fig. 6

254x190mm (72 x 72 DPI)

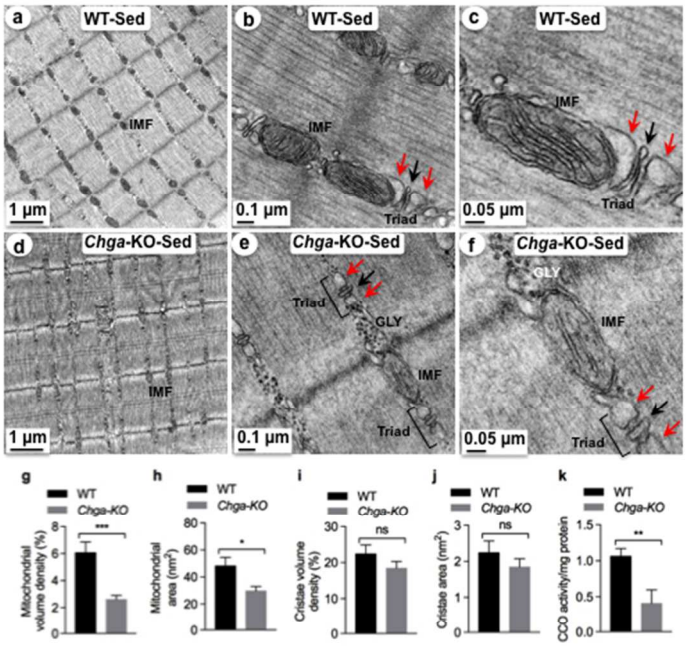

Fig. 7

254x190mm (72 x 72 DPI)

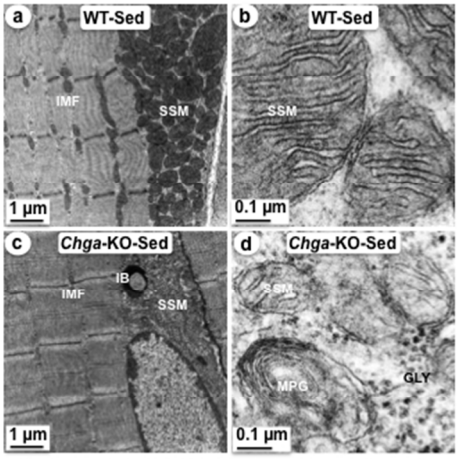

Fig. 8

254x190mm (72 x 72 DPI)

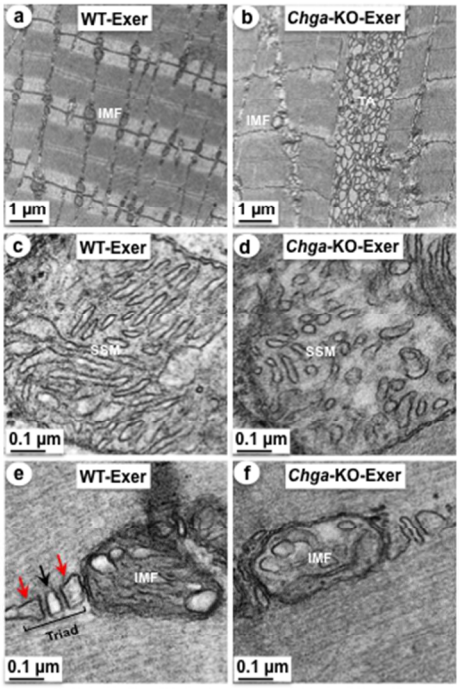

Fig. 9

254x190mm (72 x 72 DPI)

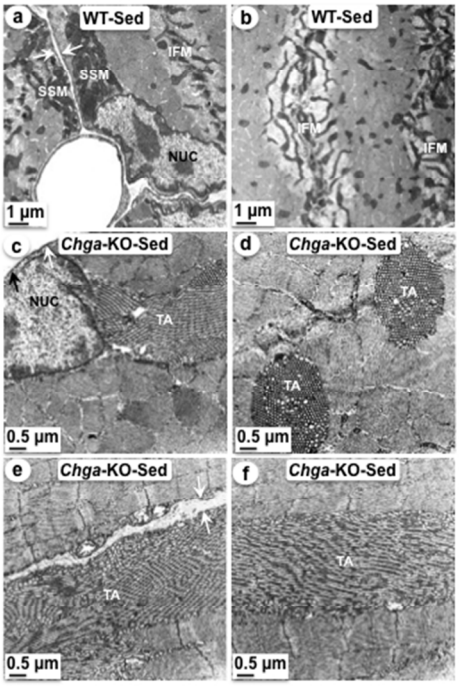

Fig. 10

254x190mm (72 x 72 DPI)

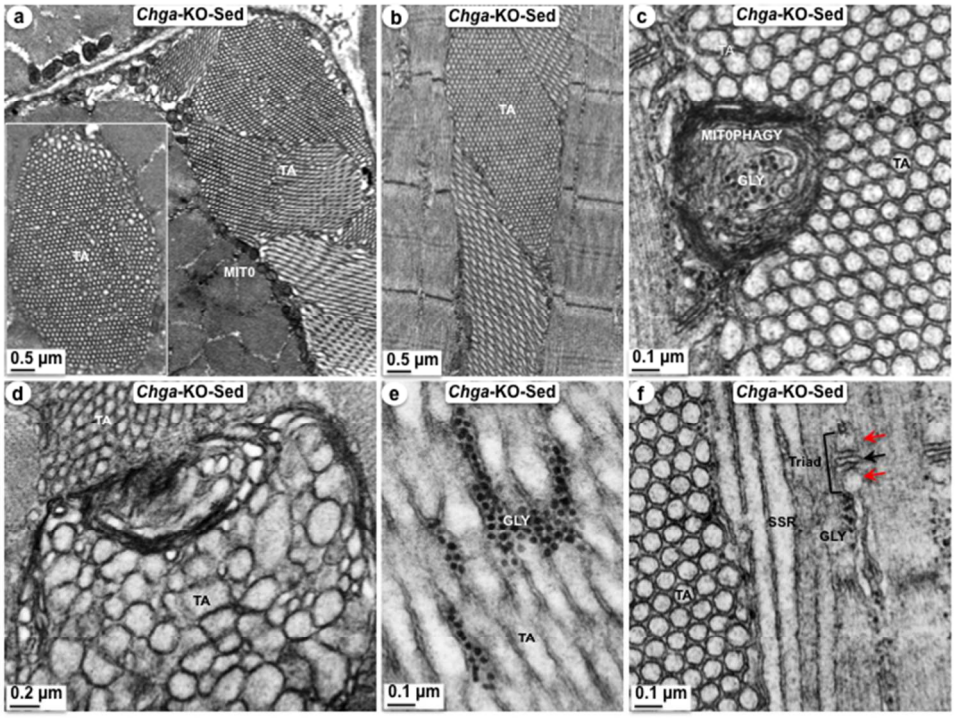

Fig. 11

254x190mm (72 x 72 DPI)

Table 1. Primer sequences for genes used in the real-time PCR analysis

Description	**Sequence 5'-3'**
Acta2/*a-Sma*-FP	TCCCAGACATCAGGGAGTAA
Acta2/*a-Sma*-RP	TCGGATACTTCAGCGTCAGGA
Cd36-FP	ATGGGCTGTGATCGGAACTG
Cd36-RP	GTCTTCCCAATAAGCATGTCTCC
Chga-FP	CCAAGGTGATGAAGTGCGTC
Chga-RP	GGTGTCGCAGGATAGAGAGGA
Chgb-FP	AGCTCCAGTGGATAACAGGGA
Chgb-RP	GATAGGGCATTTGAGAGGACTTC
Col1a1-FP	GTGCTCCTGGTATTGCTGGT
Col1a1-RP	GGCTCCTCGTTTTCCTTCTT
Col3a1-FP	GGGTTTCCCTGGTCCTAAAG
Col3a1-RP	CCTGGTTTCCCATTTTCTCC
Fn1-FP	TTGAGGAACATGGCTTTAGGC
Fn1-RP	CTGGGAACATGACCGATTTG
Fbx032/*Atrogin1*-FP	CAGCTTCGTGAGCGACCTC
Fbx032/*Atrogin1*-RP	GGCAGTCGAGAAGTCCAGTC
Gapdh-FP	AGGTCGGTGTGAACGGATTTG
Gapdh-RP	TGTAGACCATGTAGTTGAGGTCA
Slc2a4/*Glut4*-FP	ACACTGGTCCTAGCTGTATTCT
Slc2a4/*Glut4*-RP	CCAGCCACGTTGCATTGTA
Ifng-FP	ATGAACGCTACACACTGCATC
Ifng-RP	CCATCCTTTTGCCAGTTCCTC
Il1b-FP	GCAACTGTTCCTGAACTCAACT
Il1b-RP	ATCTTTTGGGGTCCGTCAACT
Il6-FP	TAGTCCTTCCTACCCCAATTTCC
Il6-RP	TTGGTCCTTAGCCACTCCTTC
Il10-FP	GCTCTTACTGACTGGCATGAG
Il10-RP	CGCAGCTCTAGGAGCATGTG
Lox-FP	TCCGCAAAGAGTGAAGAACC
Lox-RP	CATCAAGCAGGTCATAGTGG
Myf5-FP	AAGGCTCCTGTATCCCCTCAC
Myf5-RP	TGACCTTCTTCAGGCGTCTAC
Nes-FP	CCCTGAAGTCGAGGAGCTG
Nes-RP	CTGCTGCACCTCTAAGCGA
Myod1-FP	CCACTCCGGGACATAGACTTG
Myod1-RP	AAAAGCGCAGGTCTGGTGAG
Myog-FP	GAGACATCCCCCTATTTCTACCA
Myog-RP	GCTCAGTCCGCTCATAGCC
Pax3-F	CCGGGGCAGAATTACCCAC
Pax3-RP	GCCGTTGATAAATACTCCTCCG
Pax7-FP	TCTCCAAGATTCTGTGCCGAT
Pax7-RP	CGGGGTTCTCTCTCTTATACTCC

Scg2-FP	GGAGCTAAGGCGTACCGAC
Scg2-RP	TGGACATTCTCCAATCTGAGGT
Tnf-FP	CCCTCACACTCAGATCATCTTCT
Tnf-RP	GCTACGACGTGGGCTACAG
Trim63/*Murf1*-FP	GTGTGAGGTGCCTACTTGCTC
Trim63/*Murf1*-RP	GCTCAGTCTTCTGTCCTTGGA
Vegfa-FP	CTGCCGTCCGATTGAGACC
Vegfa-RP	CCCCTCCTTGTACCACTGTC